# APPLICATION OF A GENERALIZED LANGEVIN MODEL TO THE TWO-DIMENSIONAL MIXING LAYER

D. C. Haworth and S. B. Pope

Sibley School of Mechanical and Aerospace Engineering
Cornell University
Ithaca, New York 14853

## ABSTRACT

A modeled transport equation for the joint pdf of the velocities and a scalar has been solved numerically for the plane turbulent mixing layer. A generalized Langevin equation models the effects of the fluctuating pressure and viscosity, while a stochastic mixing model represents the effects of molecular diffusivity. Conditional modeling is included to account for intermittency. The calculated intermittency factor and both conditional and unconditional moments of the velocity field are compared with experimental data.

## INTRODUCTION

The one-point statistics of the self-similar plane turbulent mixing layer have been calculated by modeling and solving an evolution equation for the joint probability density function (pdf) of the velocities $\underline{U}(\underline{x},t)$ and a conserved passive scalar $\phi(\underline{x},t)$. Three terms must be modeled in the pdf evolution equation: these terms represent the effects of viscosity, the fluctuating pressure, and molecular diffusivity. A generalized Langevin equation (1) is used to close the viscosity and fluctuating pressure terms and a stochastic mixing model (2) accounts for molecular diffusivity. Intermittency is incorporated using the conserved passive scalar approach of Kollmann and Janicka (3). The resulting conditionally-modeled joint pdf evolution equation is solved by a Monte Carlo method (4).

The pdf approach is advantageous in modeling complex turbulent flows because processes such as convection, buoyancy, and reaction can be treated without approximation (4-7). For the constant-density inert mixing layer, this means that convection is treated without the usual gradient transport assumption (see Ref. 8, for example). Several calculations based on joint pdf equations have been reported in the literature both for reacting flows and for inert flows: see Pope (4) for an extensive bibliography.

The present work is an extension and improvement of previous pdf calculations (9,10). In earlier calculations of the self-similar plane jet (10), a stochastic mixing model was used to model viscous dissipation, and a stochastic reorientation model was used to model the pressure fluctuations. The reorientation model results in a linear return to isotropy for the Reynolds stresses (i.e. Rotta's model). Good agreement with experimental data was obtained in spite of the fact that the rapid-pressure terms were ignored.

The generalized Langevin model used in the present calculations is both physically more sound and of wider applicability than these earlier models: rapid-pressure effects are included and a joint-normal pdf is ensured in homogeneous turbulence, in agreement with experimental data (1). Until now, this model has been calibrated and tested only for homogeneous flows.

The solution algorithm used previously (10) is limited to calculating the self-similar solution. A new, more general, solution method is used here which allows the calculation of one-dimensional transient flows or two-dimensional stationary thin free shear flows, regardless of whether a self-preserving solution exists.

The purpose of the present investigation is two-fold. First, we wish to extend the generalized Langevin model to inhomogeneous flows. Since all the Langevin model constants have been determined previously by reference to homogeneous flows (1) and since convective transport requires no modeling, there are no additional model constants to be adjusted to match experimental data in this flow; only the turbulent time scale $\tau(\underline{x},t)$ is at our disposal. Our second goal is to test the solution algorithm. Unlike the method used previously (10), the current method is designed to solve for developing flows as well as self-similar ones.

We begin in the next section with a discussion of the closure models for the unconditional pdf evolution equation. In subsequent sections, the conditional modeling, the solution algorithm, and a comparison with experimental data are presented. A summary and conclusions appear in the final section.

## UNCONDITIONAL MODELING

We define $f(\underline{V},\psi;\underline{x},t)$ to be the joint pdf of the event $\{\underline{U}(\underline{x},t) = \underline{V},\ \phi(\underline{x},t) = \psi\}$. If $Q(\underline{U},\phi)$ is any function of $\underline{U}$ and $\phi$, the mean of Q at any $\underline{x}$ and t is given in terms of the joint pdf as

$$\langle Q(\underline{U},\phi)\rangle = \int\int Q(\underline{V},\psi) f(\underline{V},\psi)\, d\underline{V}\, d\psi. \qquad (1)$$

Here, $\int d\underline{V}$ represents integration over all velocity space and $\int d\psi$ represents integration over all composition space. In this statistically stationary two-dimensional flow, f is independent of z and t (see Fig. 1): $f = f(\underline{V},\psi;x,y)$. In the self-similar regime, a dimensionless cross-stream similarity variable $\eta$ can be introduced to reduce the dimensionality of f further: $f = f(\underline{V},\psi;\eta)$.

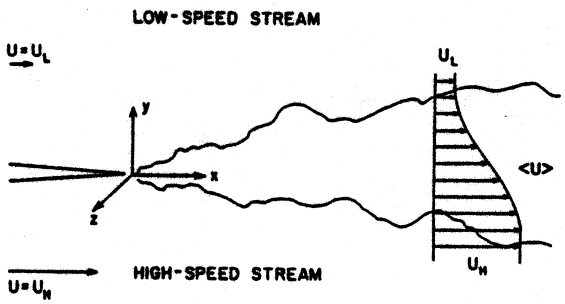


Fig. 1 The plane turbulent mixing layer.

A transport equation for the joint pdf of the velocities and scalars in a turbulent flow can be derived from the Eulerian conservation equations for $\underline{U}(\underline{x},t)$ and $\phi(\underline{x},t)$ (4, 5, 11). In a constant density flow, the terms to be modeled are those representing the effects of viscosity, the fluctuating pressure, and molecular diffusivity.

A Lagrangian approach is most expedient when modeling and solving the joint pdf equation. At time t, the position, velocity, and composition (a conserved passive scalar) of a fluid particle are denoted by $\hat{\underline{x}}(t)$, $\hat{\underline{U}}(t)$, and $\hat{\phi}(t)$.

In accordance with the Navier-Stokes equations and the conservation equation for a conserved passive scalar, the increments in $\hat{\underline{x}}(t)$, $\hat{\underline{U}}(t)$, and $\hat{\phi}(t)$ in a time interval dt are given by

$$d\hat{x}_i = \hat{U}_i dt\ , \qquad (2)$$

$$d\hat{U}_i = \left(\nu\nabla^2\langle U_i\rangle - \frac{1}{\rho}\frac{\partial\langle p\rangle}{\partial x_i}\right)dt + \left(\nu\nabla^2 u_i - \frac{1}{\rho}\frac{\partial p'}{\partial x_i}\right)dt\ , \qquad (3)$$

$$d\hat{\phi} = \Gamma\nabla^2\langle\phi\rangle dt + \Gamma\nabla^2\phi'\ dt\ . \qquad (4)$$

The Eulerian fields have been decomposed into their means $\langle\underline{U}\rangle$, $\langle p\rangle$, $\langle\phi\rangle$ and fluctuations $\underline{u}$, $p'$, $\phi'$; $\nu$ is the kinematic viscosity and $\Gamma$ is the molecular diffusivity. Closure models for the three terms to be modeled in the pdf evolution equation are constructed by modeling the corresponding terms in the Lagrangian equations, Eqs. (3) and (4).

The first two terms to be modeled represent viscosity and the fluctuating pressure. These terms are closed by modeling the corresponding terms in the Lagrangian velocity equation, Eq. (3). According to the generalized Langevin model (1), the increment in fluid particle velocity in a time interval dt is given by

$$d\hat{U}_i = \left(\nu\nabla^2\langle U_i\rangle - \frac{1}{\rho}\frac{\partial\langle p\rangle}{\partial x_i}\right)dt + G_{ij}(\hat{U}_j - \langle U_j\rangle) + (C_0\varepsilon)^{1/2}dW_i(t)\ . \qquad (5)$$

Here, $G_{ij}(\underline{x},t)$ is a function of local mean quantities, $\varepsilon(\underline{x},t)$ is the dissipation rate of turbulent kinetic energy, $C_0$ is a universal constant, and $\underline{W}(t)$ is an isotropic Wiener process. Consequently, $d\underline{W}(t)$ is a joint-normal random vector with zero mean and an isotropic covariance matrix

$$\langle dW_i(t)dW_j(t)\rangle = dt\ \delta_{ij}. \qquad (6)$$

Comparing Eq. (5) with Eq. (3), it may be seen that the terms containing $G_{ij}$ and $C_0$ model the effects of viscosity and of the fluctuating pressure.

Haworth and Pope (1) proposed a functional form for $G_{ij}$ that is linear in the mean velocity gradients $\partial\langle U_p\rangle/\partial x_q$ and in the Reynolds stresses $\langle u_k u_\ell\rangle$. The resulting model contains 11 coefficients. The value of the universal constant $C_0$ is taken to be 2.1, following Anand and Pope (12). Of the 11 model coefficients appearing in $G_{ij}$, 7 degrees of freedom are eliminated by exact constraints deduced from the Navier-Stokes equations. The remaining four coefficients (assumed constants) were determined empirically by matching the modeled evolution of the Reynolds stresses to experimental data in homogeneous turbulent flows. The values used in the present computations are identical to the optimal values given in (1).

The final term to be modeled in the pdf evolution equation represents the effects of molecular diffusivity. A stochastic mixing model is used to model this process (2,10). This model involves a constant $C_\phi$, the ratio of the velocity turbulent time scale to the scalar turbulent time scale. We take $C_\phi = 2.0$, the conventional value (10).

It remains to specify the turbulent time scale $\tau(\underline{x},t)$ where

$$\tau(\underline{x},t) \equiv \frac{k}{\varepsilon} = \frac{\langle u_i u_i\rangle}{2\varepsilon} \qquad (7)$$

In (10), it was assumed that $\tau(\underline{x},t)$ was uniform across the plane jet. The turbulent frequency $\omega(\underline{x},t) = 1/\tau(\underline{x},t)$ was related to the mean flow scales simply by

$$\omega(x) = \omega^* \frac{\Delta U}{\delta(x)}\ , \qquad (8)$$

where $\omega^*$ is a constant, $\Delta U \equiv U_H - U_L$ (Fig. 1), and $\delta(x)$ is a suitable measure of the flow width. For the plane mixing layer, we extend Eq. (8) to allow for a non-uniform turbulent frequency:

$$\omega(x,y) = \omega^*(y)\,\frac{\Delta U}{\delta(x)}\,. \qquad (9)$$

Consistent with workers presenting experimental data for the plane mixing layer (13-14), we choose

$$\delta(x) \equiv y_{.10}(x) - y_{.95}(x)\,, \qquad (10)$$

where $y_{.10}(x)$ is the lateral position at which $\langle U\rangle - U_L$ is equal to .10 $\Delta U$, and $y_{.95}(x)$ is defined analogously.

Two sets of calculations are reported. In the first, we choose a constant value for $\omega^*$, $\omega^* = 0.18$, approximately the value at $y = y_{.50}$ in the data of Wygnanski and Fiedler (13).

In the second set of calculations, $\omega^*$ varies across the layer. The dimensionless cross-stream similarity variable $\eta$ is defined by

$$\eta \equiv \frac{y - y_{.50}(x)}{\delta(x)} = \frac{y - y_{.50}(x)}{y_{.10}(x) - y_{.95}(x)}\,. \qquad (11)$$

The data of Wygnanski and Fiedler show that $\omega^*$ varies by about a factor of 2 across the flow, monotonically increasing from the high-speed side to the low-speed side. As a crude approximation, we take $\omega^*(\eta)$ to be piecewise linear: $\omega^*(\eta) = 0.135$ for $\eta < -.25$; $\omega^*(\eta) = 0.18(1+\eta)$ for $-.25 < \eta < 0.50$; and, $\omega^*(\eta) = 0.27$ for $\eta > 0.50$.

## CONDITIONAL MODELING

To incorporate the effect of intermittency, we adopt the conserved passive scalar approach introduced by Kollmann and Janicka (3). A scalar $\phi(\underline{x},t)$ takes on values of one in the high-speed irrotational stream and zero in the low-speed irrotational stream. The condition $\{0 < \phi(\underline{x},t) < 1\}$ is then used to distinguish turbulent fluid from nonturbulent fluid. The intermittency factor $\gamma(\underline{x},t)$ is defined as the probability of the fluid being turbulent. In terms of $\phi(\underline{x},t)$, then, the intermittency factor is given by

$$\gamma(\underline{x},t) = \text{Prob}\{0 < \phi(\underline{x},t) < 1\}\,. \qquad (12)$$

The conditional modeling used here is in most respects identical to that used previously by Pope (10). Three model constants $C_g$, $C_m$, and $C_e$ are introduced which control, respectively, the rate of entrainment of nonturbulent fluid, the rate of momentum transfer between turbulent and nonturbulent fluid, and the rate of energy transfer between turbulent and nonturbulent fluid. We take the same values as were used for the plane jet (10): $C_g = 1.5$, $C_m = 1.5$, and $C_e = 5.0$.

The current modeling departs from the earlier work in one respect: no attempt is made to account for the effects of the fluctuating pressure on the nonturbulent fluid. While pressure fluctuations do occur in the nonturbulent fluid, the resulting velocity fluctuations have little overall effect on the flow. In (10), it was shown that the energy in the nonturbulent velocity fluctuations is quite small compared to the energy in the turbulent velocity fluctuations for most thin free shear flows. As we are not interested in the nonturbulent fluctuations themselves but only in their effects on the flow as a whole, the simplified approach taken here appears to be justified.

## SOLUTION ALGORITHM

The Monte Carlo solution algorithm is discussed in detail in (4), and is presented here in outline form only.

In the Monte Carlo method, the joint pdf is represented by a large number N of notional particles. At time t, the $n^{th}$ particle has position $\underline{x}^{(n)}(t)$, velocity $\underline{U}^{(n)}(t)$, and composition $\phi^{(n)}(t)$. The state of each particle $[\underline{x}^{(n)}, \underline{U}^{(n)}, \phi^{(n)}]$ evolves in time according to the modeled Lagrangian equations. For the current calculations, this means that the position and velocity of each particle change in accordance with the generalized Langevin equation (Eqs. 2 and 5) while the composition changes in accordance with the stochastic mixing model (2,4).

A significant simplification is afforded by requiring that there be negligible probability of a particle having a negative streamwise velocity. This permits the use of an explicit marching scheme to advance the solution in the streamwise direction from given initial conditions. A consequence of this restriction in modeling the plane mixing layer is that the mean velocity of the low speed stream must be positive. Thus, while we compare our calculations with experimental data for which $U_L$ is essentially zero, in the computations a finite velocity ratio $U_H/U_L$ must be specified. We choose $U_H/U_L = 10$, a value that should be sufficiently large that the self-similar solution does not differ significantly from the case $U_H/U_L = \infty$, yet sufficiently small that the numerical solution is not degraded.

Further simplifications arise from invoking the boundary-layer assumption: only the dominant mean velocity gradient term $\partial\langle U\rangle/\partial y$ is retained in $G_{ij}$ and the cross-stream mean momentum equation reduces to an equation for the mean pressure gradient (15):

$$\frac{\partial\langle p\rangle}{\partial y} = -\rho\,\frac{\partial\langle v^2\rangle}{\partial y}\,. \qquad (13)$$

The term $\nu\nabla^2\langle U_i\rangle$ is neglected in Eq. (5) due to high Reynolds number, and unconditional averages are used to form $G_{ij}$. However, the mean velocity conditional on the fluid being turbulent is used in the linear deterministic term of the Langevin equation (the second term on the right-hand side of Eq. 5): this term represents a linear motion (in velocity space) about the local turbulent mean velocity.

Eulerian means are extracted from the numerical solution using cross-validated least squares cubic splines as described in (4); the statistical error in this procedure is of order $N^{-1/2}$. The calculations reported here are for N = 20,000. No averaging over steps is used for the calculated profiles presented in the next section, since we want to demonstrate that the solution algorithm is applicable to developing flows as well as to self-similar flows.

## RESULTS AND DISCUSSION

Many experimental results have been reported for the plane turbulent mixing layer beginning with Liepmann and Laufer (16) whose 1947 paper provided the benchmark for subsequent experiments. We limit our attention to those in which the velocity ratio $U_H/U_L$ is infinite. The most comprehensive measurements available are those of Wygnanski and Fiedler (13) and Champagne, Pao, and Wygnanski (14).

There is wide scatter in the data among the various experiments. All achieve a self-similar state with linear spread of the mixing layer as predicted by simple scaling arguments (15). However, taking as a measure of the spreading rate the quantity $\delta'$

$$\delta' = \frac{y_{.10}(x) - y_{.95}(x)}{x - x_0} \qquad (14)$$

where $x_0$ is the virtual origin of the flow, it is observed (14) that $\delta'$ varies from 0.17 for Liepmann and Laufer to 0.23 for Wygnanski and Fiedler. The peak streamwise turbulence intensity $\langle u^2\rangle^{1/2}/U_H$ varies from 0.15 to 0.18 in these same experiments, with similar scatter evident in the other Reynolds stress components. The origin of these differences presumably lies in the initial conditions, boundary conditions, and Reynolds number of the flow (14), factors which are beyond the scope of our modeling.

Using the models and solution method described above, the calculations yield a self-preserving solution with linear growth of the mixing layer. The computed spreading rate is $\delta' = 0.050$ for uniform $\omega^*$ and $\delta' = 0.048$ for piecewise linear $\omega^*$. This is smaller by a factor of 4 than experiments with $U_H/U_L = \infty$ indicate. Taking into account the effect of finite velocity ratio on spreading rate (17), it is about one-third of the growth rate expected for a velocity ratio of 10. A discussion of this low spreading rate follows the comparison of calculated profiles with experimental data. Use of the normalized cross-stream similarity variable $\eta$ (Eq. 11) removes the effect of spreading rate in these comparisons.

Profiles of the normalized mean streamwise velocity and the intermittency factor are shown in Fig. 2. The calculated mean velocity profile is in good agreement with experimental data for the uniform $\omega^*$ case, while there is significant disagreement at both edges of the flow for the piecewise linear $\omega^*$ case. By contrast, the computed intermittency factor appears to be better for piecewise linear $\omega^*$. The calculations indicate a turbulent zone which extends markedly too far into the low-speed stream in both cases.

Figure 2 illustrates the sensitivity of the calculations to the assumed turbulent frequency $\omega(\underline{x},t)$. All subsequent figures show only the uniform $\omega^*$ calculations, for which the normalized mean velocity profile agrees with experimental data.

The conditional and unconditional mean streamwise velocities are shown in Fig. 3: $\langle U\rangle_T$ is the mean velocity conditional on the fluid being turbulent, and $\langle U\rangle_N$ is the mean velocity conditional on the fluid being nonturbulent. The computed behavior of $\langle U\rangle_N$ appears to be qualitatively correct near the edges of the layer, with $\langle U\rangle_N > \langle U\rangle$ on the high-speed side and $\langle U\rangle_N < \langle U\rangle$ on the low-speed side. However, the behavior of $\langle U\rangle_T$ implies a serious defect in the conditional modeling. The experimental data indicate that the "slip" velocity $\langle U\rangle_T - \langle U\rangle$ is nearly equal to zero on the high-speed side of the flow and is large on the low-speed side, while the model produces the opposite behavior.

Calculated and experimental profiles of the Reynolds stresses are shown in Figs. 4-7. The overall turbulent kinetic energy level is different for the computations and for the two sets of experimental data. Each profile is thus normalized by the peak turbulent kinetic energy for that computation or experiment. Values of these normalization factors $k_{max}/\Delta U^2$ are as follows:

| | |
|---|---|
| uniform $\omega^*$ computation | 0.0204 |
| Champagne et al. (14) | 0.0290 |
| Wygnanski and Fiedler (13) | 0.0358. |

Figures 4-7 show that the model puts too much energy into the streamwise fluctuations $\langle u^2\rangle$ at the expense of the cross-stream fluctuations $\langle v^2\rangle$. The calculated peak of $\langle uv\rangle/k_{max}$ is lower than experimental data indicate, and the calculated profiles of $\langle v^2\rangle$ and $\langle w^2\rangle$ are shifted towards the low-speed stream.

We seek some understanding of the model's behavior and how it might be improved. This is achieved by examining the effect of the normalized Reynolds stresses $\langle u_i u_j\rangle/k$ on the spreading rate and on the production of k and of $\langle uv\rangle/k$. By invoking the boundary-layer assumption in the mean streamwise momentum equation, we see that the spreading rate $\delta'$ scales as $\langle uv\rangle/\Delta U^2$ (15). Similarly, the ratio of production to dissipation of turbulent kinetic energy $P/\varepsilon$ scales as $\langle uv\rangle\Delta U/(k\omega\delta) = (1/\omega^*)(\langle uv\rangle/k)$; and the dominant production term in the evolution equation for $\langle uv\rangle/k$ is $-(\langle v^2\rangle/k)\partial\langle U\rangle/\partial y$. Consider now starting the calculations with the correct mean-velocity and turbulent kinetic energy profiles, but with $\langle u^2\rangle/k$ being too large and, more important, $\langle v^2\rangle/k$ being too small. First, since the production of $\langle uv\rangle$ $(-\langle v^2\rangle\partial\langle U\rangle/\partial y)$ is too small, $\langle uv\rangle$ becomes too small. Then with $P/\varepsilon = (1/\omega^*)\langle uv\rangle/k$ being too small, k becomes too small. And also, the too small value of $\langle uv\rangle$ causes the spreading rate $\delta'$ to be too small. It may be seen, then, that all the deficiencies in the calculations can be attributed to the model's making $\langle v^2\rangle/k$ too small.

It remains to understand why the computations yield too small a value of $\langle v^2\rangle/k$. A possible hypothesis is that the plane mixing layer is significantly different from the homogeneous shear flows used to calibrate the Langevin model. The difference could either be in the normalized shear rate $T^* \equiv \tau\,\partial\langle U\rangle/\partial y$, or in the fact that the mixing layer is inhomogeneous. The first explanation can readily be dismissed: the mixing-layer data of Wygnanski and Fiedler give $T^* = 5.6$ in the middle of the layer, which is close to the values $T^* = 5.7$ and $T^* = 6.1$ in the homogeneous shear flows (18,19) used to calibrate the model.

Compared to homogeneous shear flows, the inhomogeneous mixing layer contains several different physical phenomena. But, in the fully-turbulent center of the mixing layer, the only difference in the modeled joint pdf equation is the convective transport—which is treated exactly. Evidently the effect of this transport is small: in the mixing layer we calculate $(\langle v^2\rangle/k\text{-}2/3) = -0.32$ whereas in the homogeneous shear flow the value is $(\langle v^2\rangle/k\text{-}2/3) = -0.30$. In the exact pdf equation there is a transport term associated with pressure fluctuations. It is possible that the inclusion of a model for this term would augment the transport and reduce the anisotropy. This is a topic for future investigation.

## SUMMARY AND CONCLUSIONS

A conditionally-modeled joint pdf evolution equation has been solved by a Monte Carlo method to calculate the one-point statistics of a self-similar plane mixing layer. Two new features of these calculations are the use of a generalized Langevin

model and the introduction of a new solution algorithm.

Based on these calculations, we conclude that both the Langevin model and the solution algorithm are working properly. The plane jet calculations of Pope (10) were repeated using the current solution algorithm and the results were similar to those reported in (10), thus strengthening the second conclusion.

These calculations have also pointed out weaknesses in the modeling which must be addressed. First, an understanding is needed of the differences among flows which had been thought to be similar. In particular, differences must be understood among homogeneous shear flows, the plane jet (for which the conditional modeling used here appeared to be adequate, 10), and the plane mixing layer. Second, the conditional modeling must be improved and generalized to work in a variety of flows. Third, the modeling of the turbulent frequency $\omega(\underline{x},t)$ or equivalently, the dissipation rate $\varepsilon(\underline{x},t)$ needs to be improved and generalized. Current efforts in this direction treat $\varepsilon$ as a random variable and solve a modeled evolution equation for the joint pdf of the velocities, scalars, and the dissipation (20). In addition, we seek to increase the efficiency and accuracy of the solution method by introducing a second-order accurate scheme to advance the solution in x (21).

REFERENCES


1 Haworth, D.C. and Pope, S.B., "A Generalized Langevin Model for Turbulent Flows," submitted to Physics of Fluids, 1985.

2 Pope, S.B., "An Improved Turbulent Mixing Model," Combustion Science and Technology, Vol. 28, 1982, pp. 131-145.

3 Kollmann, W. and Janicka, J., "The Probability Density Function of a Passive Scalar in Turbulent Shear Flows," Physics of Fluids, Vol. 25, No. 10, October 1982, pp. 1755-1769.

4 Pope, S.B., "PDF Methods for Turbulent Reactive Flows," Progress in Energy and Combustion Science, 1985 (to be published).

5 Pope, S.B., "Transport Equation for the Joint PDF of Velocity and Scalars in a Turbulent Flow," Physics of Fluids, Vol. 24, No. 4, April 1981, pp. 588-596.

6 Lundgren, T.S., "Model Equation for Nonhomogeneous Turbulence," Physics of Fluids, Vol. 12, No. 3, March 1969, pp. 485-497.

7 Dopazo, C., "A Probabilistic Approach to Turbulent Flame Theory," Acta Astronautica, Vol. 3, 1976, pp. 853-878.

8 Lumley, J.L., "Computational Modeling of Turbulent Flows," Advances in Applied Mechanics, Vol. 18, 1978, pp. 123-176.

9 Pope, S.B., "Calculations of Velocity-Scalar Joint PDF's," Turbulent Shear Flows III, Bradbury, L.J.S., et al. (eds.), Springer-Verlag, Heidelberg, 1983, pp. 113-123.

10 Pope, S.B., "Calculations of a Plane Turbulent Jet," AIAA Journal, Vol. 22, No. 7, July 1984, pp. 896-904.

11 Lundgren, T.S., "Distribution Functions in the Statistical Theory of Turbulence," Physics of Fluids, Vol. 10, No. 5, May 1967, pp. 969-975.

12 Anand, M.S. and Pope, S.B., "Diffusion Behind a Line Source in Grid Turbulence," Turbulent Shear Flows IV, Bradbury, L.J.S., et al. (eds.), Springer-Verlag, Heidelberg, 1984, pp. 46-61.

13 Wygnanski, I. and Fiedler, H.E., "The Two-Dimensional Mixing Region," Journal of Fluid Mechanics, Vol. 41, Part 2, 1970, pp. 327-361.

14 Champagne, F.H., Pao, Y.H. and Wygnanski, I.J., "On the Two-Dimensional Mixing Region," Journal of Fluid Mechanics, Vol. 74, Part 2, 1976, pp. 209-250.

15 Tennekes, H. and Lumley, J.L., A First Course in Turbulence, MIT Press, Cambridge, 1972.

16 Liepmann, H.W. and Laufer, J., "Investigation of Free Turbulent Mixing," N.A.C.A. TN1257, 1947.

17 Masutani, S.M., "An Experimental Investigation of Mixing and Chemical Reaction in a Plane Mixing Layer," Ph.D. Thesis, Stanford University, March 1985.

18 Harris, V.G., Graham, J.A.H. and Corrsin, S., "Further Experiments in Nearly Homogeneous Turbulent Shear Flow," Journal of Fluid Mechanics, Vol. 81, Part 4, 1977, pp. 657-687.

19 Tavoularis, S. and Corrsin, S., "Experiments in Nearly Homogeneous Turbulent Shear Flow with a Uniform Mean Temperature Gradient. Part 1," Journal of Fluid Mechanics, Vol. 104, 1981, pp. 311-347.

20 Pope, S.B. and Haworth, D.C., "The Mixing Layer Between Turbulent Fields of Different Scales," to be presented at Fifth Symposium on Turbulent Shear Flows, August 1985.

21 Pope, S.B. and Haworth, D.C., "A Second Order Monte Carlo Method for the Solution of a Generalized Langevin Equation," in preparation, 1985.

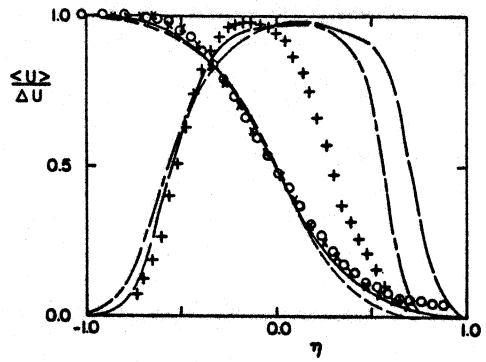


Fig. 2 Normalized mean velocity and intermittency.

——— $\langle U\rangle/\Delta U$, uniform ω* calculation
– – – $\langle U\rangle/\Delta U$, piecewise linear ω* calculation
— — $\gamma$, uniform ω* calculation
– – – $\gamma$, piecewise linear ω* calculation
X $\langle U\rangle/\Delta U$, Wygnanski and Fiedler (13)
0 $\langle U\rangle/\Delta U$, Champagne et al. (14)
\+ $\gamma$, Wygnanski and Fiedler

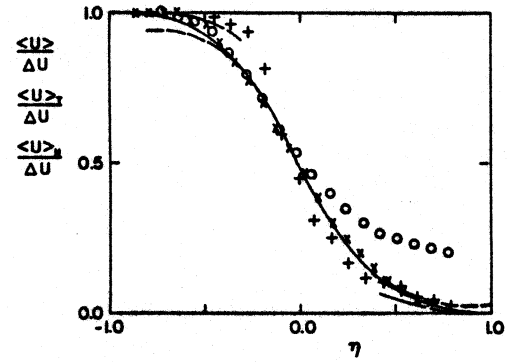


Fig. 3 Conditional and unconditional mean velocities.

——— $\langle U\rangle/\Delta U$, uniform ω* calculation
– – – $\langle U\rangle_T/\Delta U$, uniform ω* calculation
— — $\langle U\rangle_N/\Delta U$, uniform ω* calculation
X $\langle U\rangle/\Delta U$, Wygnanski and Fiedler
0 $\langle U\rangle_T/\Delta U$, Wygnanski and Fiedler
\+ $\langle U\rangle_N/\Delta U$, Wygnanski and Fiedler

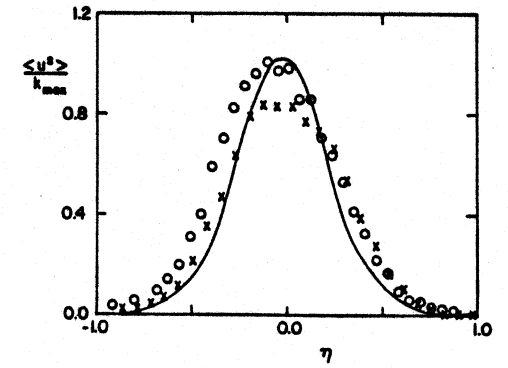


Fig. 4 Normalized streamwise velocity fluctuations.

——— $\langle u^2\rangle/k_{max}$, uniform ω* calculation
X $\langle u^2\rangle/k_{max}$, Wygnanski and Fiedler
0 $\langle u^2\rangle/k_{max}$, Champagne et al.

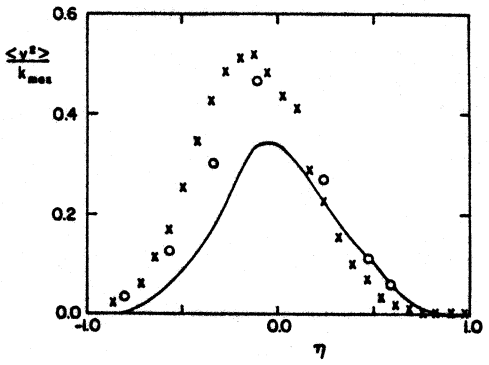


Fig. 5 Normalized lateral velocity fluctuations.

——— $\langle v^2\rangle/k_{max}$, uniform ω* calculation
X $\langle v^2\rangle/k_{max}$, Wygnanski and Fiedler
0 $\langle v^2\rangle/k_{max}$, Champagne et al.

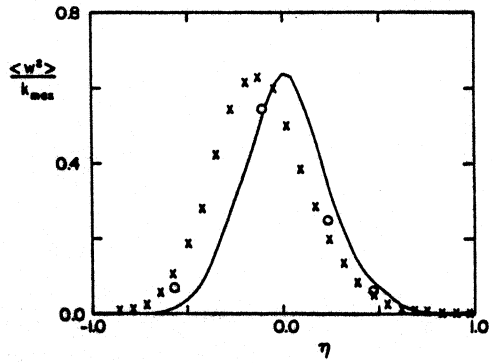


Fig. 6 Normalized transverse velocity fluctuations.

——— $\langle w^2\rangle/k_{max}$, uniform ω* calculation
X $\langle w^2\rangle/k_{max}$, Wygnanski and Fiedler
0 $\langle w^2\rangle/k_{max}$, Champagne et al.

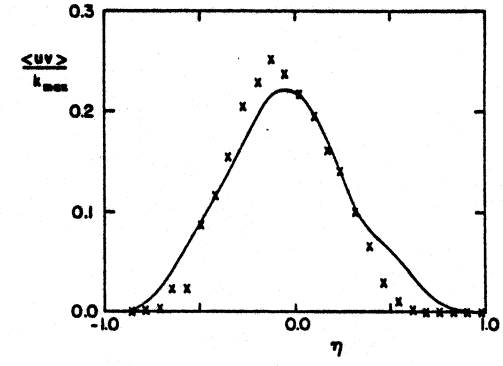


Fig. 7 Normalized shear stress.

——— $\langle uv\rangle/k_{max}$, uniform ω* calculation
X $\langle uv\rangle/k_{max}$, Wygnanski and Fiedler